Cage-Embedded Crown-Type Dual Coil Wireless Power Transfer Based Microwave Brain Stimulation System for Untethered and Moving Mice

Jinhyun Kim, *Graduate Student Member, IEEE*, Sanggeon Park, Seongwoog Oh, *Graduate Student Member, IEEE*, Yeowool Huh, Jeiwon Cho, and Jungsuek Oh, *Senior Member, IEEE*

***Abstract*—This study proposes a novel brain-stimulated mouse experiment system which is insensitive to the variations in the position and orientation of a mouse. This is achieved by the proposed novel crown-type dual coil system for magnetically coupled resonant wireless power transfer (MCR-WPT). In the detailed system architecture, the transmitter coil consists of a crown-type outer coil and a solenoid-type inner coil. The crown-type coil was constructed by repeating the rising and falling at an angle of 15° for each side which creates the H-field diverse direction. The solenoid-type inner coil creates a magnetic field distributed uniformly along the location. Therefore, despite using two coils for the Tx system, the system generates the H-field insensitive to the variations in the position and angle of the receiver system. The receiver is comprised of the receiving coil, rectifier, divider, LED indicator, and the MMIC that generates the microwave signal for stimulating the brain of the mouse. The system resonating at 2.84 MHz was simplified to easy fabrication by constructing 2 transmitter coils and 1 receiver coil. A peak PTE of 19.6% and a PDL of 1.93 W were achieved, and the system also achieved an operation time ratio of 89.55% in vivo experiments. As a result, it is confirmed that experiments could proceed for approximately 7 times longer through the proposed system compared to the conventional dual coil system.**

***Index Terms*—Wireless power transfer, brain stimulation system, biomedical applications, magnetic coupling resonance, near-field coupling.**

Manuscript received 25 October 2022; revised 24 December 2022, 2 January 2023, and 20 February 2023; accepted 4 March 2023. Date of publication 10 March 2023; date of current version 19 May 2023. This work was supported in part by the National Research Foundation of Korea (NRF) funded by the Ministry of Science and ICT under Grants NRF-2018M3C7A1024736, NRF-2022M3E5E8018421, and NRF-2022R1A2C2009265, and in part by the Creative-Pioneering Researchers Program through Seoul National University (SNU). The first two authors contributed equally to this work. This paper was recommended by Associate Editor M. Ghovanloo. *(Jinhyun Kim and Sanggeon Park contributed equally to this work.) (Corresponding author: Jungsuek Oh.)*

This work involved human subjects or animals in its research. Approval of all ethical and experimental procedures and protocols was granted by (Name of Review Board or Committee) (IF PROVIDED under Application No. xx, and performed in line with the (Name of Specific Declaration).

Jinhyun Kim, Seongwoog Oh, and Jungsuek Oh are with the Department of Electrical and Computer Engineering (ECE), Institute of New Media and Communications (INMC), Seoul National University, Seoul 151-742, Republic of Korea (e-mail: jinhyun111@snu.ac.kr; ohseongwoog@gmail.com; jungsuek@snu.ac.kr).

Sanggeon Park and Jeiwon Cho are with the Department of Brain and Cognitive Sciences, Scranton College and the Brain Disease Research Institute, Ewha Brain Institute, Ewha Womans University, Seoul 03760, Republic of Korea (e-mail: chalspark.korea@gmail.com; jelectro21@ewha.ac.kr).

Yeowool Huh is with the Department of Medical Science, College of Medicine, Catholic Kwandong University, Gangwon-do 210-701, Republic of Korea (e-mail: huh06@cku.ac.kr).

Color versions of one or more figures in this article are available at https://doi.org/10.1109/TBCAS.2023.3255248.

Digital Object Identifier 10.1109/TBCAS.2023.3255248

I. Introduction

WIRELESS power transfer (WPT) techniques, transferring electric power without any cables and contacts, have long been researched for contactless battery charging for smart phones and biomedical implants [1], [2], [3], [4], [5], [6]. Especially, WPT is an attractive candidate to operate biomedical implant devices without any surgery [7], [8], [9], [10]. Generally, WPT can be divided into 3 types based on the effective transfer distance: far-field energy transfer [11], near-field inductively coupled power transfer (ICPT) [12], and near-field power transfer with magnetically coupled resonant (MCR-WPT) [13], [14]. The far field radiation effect of electromagnetic waves can transfer energy over a long distance due to a low atmospheric loss. However, this type of WPT has a limitation in biomedical applications because of the power efficiency problems and fatal damage to living organisms. ICPT based on the magnetic coupling is the most commercialized WPT method at present, such as in battery charging and industrial heaters. However, ICPT also has a critical drawback concerning its range. With this method, it can only transfer electrical power up to a few cm. Interestingly, in the case of MCR-WPT, it not only transfers power over a few meters but also has high efficiency and power transmission. For these reasons, much research has progressed on MCR-WPT in the biomedical area compared to the other types due to the advantages of its transfer distance and efficiency [15], [16], [17], [18], [19], [20].

Generally, brain stimulation techniques can be divided into invasive types and non-invasive types. Especially, the non-invasive types of brain stimulation, such as transcranial direct current stimulation (tDCS), transcranial magnetic stimulation (TMS), and microwave brain stimulation (MBS), do not require any surgical operations; thus, the non-invasive type is becoming more preferred. Before a new stimulation method could be applied to humans, reliable animal experiments are essential to validate the effect of the stimulation and its safety [21], [22], [23], [24], [25]. To increase the accuracy of the experimental results during these experiments, various behaviors such as locomotion, sleep,

and feeding behaviors should not be obstructed. Moreover, it is important to minimize the stress on the animal during the experiment. However, if power for the stimulator, a device used to stimulate the brain, is supplied with cables; the behavior of the animals is constrained. Behavioral constraints could act as a stress factor for animals and interfere with the interpretation of the brain stimulation effects. In regard to reducing the stress on the animal by removing the cable, WPT has been suggested as one way to solve this problem. However, in most cases, the system driven by WPT is bulky and heavy for operating the implementer; therefore, the system still limits the movable radius of the animals. Furthermore, when the animal behaves freely, the amount of power transferred through WPT changes extremely with the free movements of the animal, and the device might not even work. Therefore, it is essential to develop a system that can ensure the free behavior of animals and transfer power constantly. In other words, the transmit power should be independent of the position and orientation of the receiving system. Various topologies for implementing WPT systems have been proposed to overcome these problems [26], [27], [28], [29], [30], [31], [32], [33], [34], [35], [36], [37], [38], [39], [40], [41], [42], [43]. The first topology is to arrange the multiple transmitter (Tx) coils in the omnidirectional [26], [27], [28], [29], [30], [31], [32], [33]. In this case, irrespective of the position and orientation of the receiver (Rx), almost uniform power can be delivered from the Tx. However, the size of the Tx coils should be increased, and the system function based on the mutual inductance of multiple coils. Due to the multiple coils in the Tx system; thus, the system complexity is increased, and the system performance relies on the fabrication experiment results. Moreover, the input power is divided into each coil; thus, the efficiency of the system is decreased, and the system is not suitable for a high-power transfer system. In the second topology, the Rx coil can be arranged omnidirectionally with a single Tx coil [34], [35], [36], [37], [38], [39]. If the system design generates a sufficient magnetic field for WPT, the transmission power is insensitive to changes in the angle of the Rx. Nevertheless, the weight and volume of the Rx are essentially expanded because the amount of the coil is increased, and an additional structure is needed to fix the Rx coil. Thus, the behavior of the animals is limited by the heavy weight. The last method is to utilize embedded coils, such as bowl type, butterfly type, and anchor type [40], [41], [42], [43]. This method can generate a uniform magnetic field regardless of the Rx position and rotation. However, the embedded coils have the issue that it is hard to fabricate due to the unique coil design.

In this study, we proposed an embedded coil MCR-WPT system that is insensitive to variations in position and can transfer power even if the alignment of the Tx and Rx coil is tilted. The proposed embedded coil, a crown-type dual coil, is designed to be less affected by the movement of the Rx system and enables the transmission of power with high efficiency. Moreover, the Tx coil is constructed with just 2 coils; thus, so the complexity of the Tx system is minimized and easy to fabricate. The Rx used a single coil to reduce the weight and decrease the stress on a mouse. For accurate measurement, the contactless measurement method has been proposed, and based on this, the performance of the WPT system can be evaluated accurately.

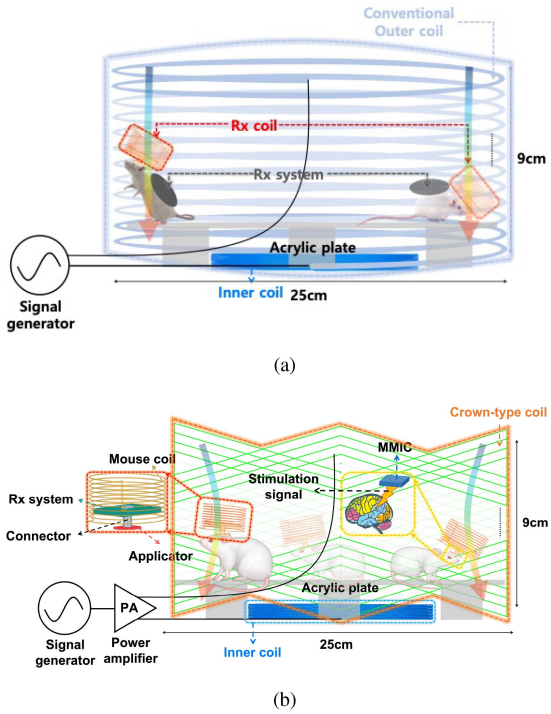

Fig. 1. The WPT system design view for small animal experiment (a) The diagram of the conventional WPT system (b) The diagram of the proposed WPT system.

II. Design of the Asymmetric Dual Coil

A. The Conventional Type of WPT Coil Design

Fig. 1(a) shows the coil design view of a conventional brain stimulation system based on the WPT. This system structure was designed based on a magnetic resonance imaging (MRI) machine configuration. An internal coil exists inside a large external coil, called an outer coil. The Rx part consists of an Rx coil for receiving the power and an Rx system to generate a stimulation signal on the back of the mouse. On the other hand, the proposed crown-type dual coil system is composed of a crown-type outer coil as shown in Fig. 1(b). Moreover, the Rx part consists of a mouse coil, printed circuit board (PCB) for placing components such as a rectifier, resistive voltage divider, MMIC, SMP connector, and applicator for stimulation by a generated signal from the chip. To begin with, to create a free behavior area, the diameter of the outer coil should be larger than 250 mm. Based on the outer coil design, the mouse coil is fabricated. The diameter of the mouse coil is 2.5 cm, and the number of turns is 10. The spacing of each turn is minimized. To prevent interference from the small animal, the Rx system must be not contacted and damaged by mouse movement. Due to the Rx system module size, the receiving coil is hard to attach laterally to the Rx system to prevent damage from the mouse moving. Thus, the receiving coil is fabricated to surround the

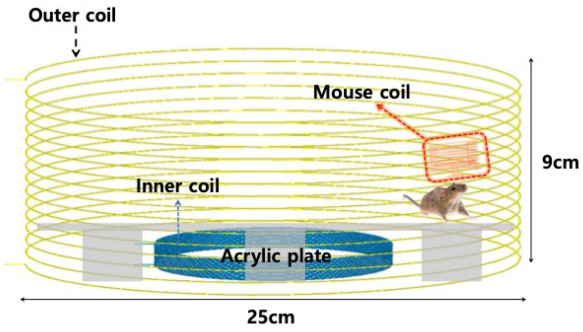

Fig. 2. Dual coil system added to the inner coil type of a WPT coil design; 3D design view.

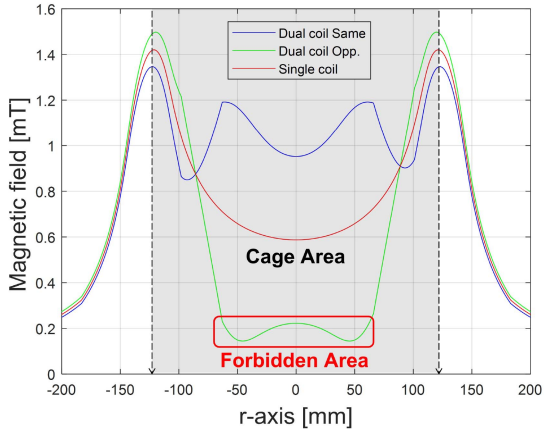

Fig. 3. Comparison of the magnetic field of a single coil, same direction dual coil, and opposite direction dual coil.

receiving system. Furthermore, MMIC also can be damaged due to mouse movement, so the receiving coil protects the MMIC by surrounding the receiving system.Moreover, the Rx system is designed to weigh less than 7 g so as not to affect the movement of the mouse. Because the Rx can attach to the head of small animals, the Rx part is located about 3 cm above the ground in the simulation. Next, the diameter, height, and spacing between each turn are established by the design parameters used to make the outer coil. Because the system uses a resonance type of WPT, the mouse coil and the outer coil should resonance at the same frequency. However, the capacitors used have 10 % tolerance and their effect has a very large effect on changing the resonance of the outer coil compared to the mouse coil. Because of this reason, the outer coil inductance has a dominant influence in setting the resonance condition.

The 3D layout of the conventional dual coil system is shown in Fig. 2. In this design, the auxiliary coil, which is called an inner coil, is added inside the outer coil, and this inner coil is connected in parallel with the outer coil. Thus, the inner coil can make an additional magnetic field in the center of the outer coil, and this magnetic field can secure the power transfer area, which was an issue for the single outer coil. Moreover, the total inductance and resistance of the Tx in the dual coil types are smaller than the conventional type due to the parallel connection. For this reason, it makes it much easier to match the Tx and Rx resonance.

In the dual coil fabrication, the analysis of the H-field is calculated based on the elliptic integral using the MATLAB 2021a Program [44], [45]. The inner coil can be wound in the same way as the outer coil, or in the opposite direction. In the opposite case, the magnetic field is combined with the outer coil magnetic field of outside the inner coil and subtracted from the two fields inside the inner coil. Because of the cancellation of the magnetic fields of the outer and inner coils, a forbidden area is generated where the summation of the magnetic fields becomes close to 0 in the inner coil area. In contrast to the opposite case, when the inner coil is wound in the same direction as the outer coil, the sum of the magnetic field is observed inside of the inner coil, and the deduction of the field is generated from outside the inner coil. Although the cancellation of the magnetic field occurs outside the inner coil, the strength of the outer coil magnetic field is increased toward the edge; thus, the forbidden area can be eliminated.

Fig. 3. shows the comparison results of the H-field simulation of a single outer coil and dual coil wound in the same direction and the opposite case. In the opposite case, the strength of the magnetic field became very weak around the 60 mm point due to the cancellation of the magnetic field from the outer coil and inner coil. However, on the edge of the outer coil, it was verified that the strength of the magnetic field becomes stronger due to the summation of the inner coil magnetic field. In contrast, the H-field is weaker at the edge of the outer coil, and the magnetic field is stronger at the center in the same direction case. Therefore, to form a uniform magnetic field distribution based on the above analysis results, the inner coil in the same direction is adopted.

To fabricate the Tx system, 3 parameters which are a radius, spacing, and turns of the outer coil and the inner coil were established. These two coils are connected in parallel and optimized to generate a uniform magnetic field. Each type of self-inductance and mutual inductance was investigated using the Q3D Extractor in ANSYS, and most tissues of a mouse are modeled to be non-magnetic tissues biologically, so the permeability of the mouse can be regarded to μ_0 [46]. Based on the extracted parameters, it implements a full circuit simulation taking into consideration the signal generation chip utilized in the ADS simulator in Agilent.

By optimization, the dual coil is fabricated such that the diameter of the outer coil is 250 mm, the spacing is 6 mm and the number of turns is 15. Moreover, the diameter of the inner coil is fixed to 120 mm and 15 turns when the mouse coil diameter is 3.5 cm, and the number of turns is 20 with minimized spacing. By utilizing the optimized inductance, one of the WPT efficiency parameters, kQ-product, is calculated to check the efficiency variation along with the Rx coil movements [47], [48], [49]. The total WPT system diagram and the equivalent circuit of the proposed system are illustrated in Fig. 4. When the Rx system is changed in its position and angle, the self inductance and its resistance are almost constant, but the mutual inductance is dominantly changed. Moreover, the input impedance, Z_{in}, is related to the transferred power from the Tx system due to the fact that the consumption current of the chip is defined along the applied voltage. Therefore, the WPT system can be simplified

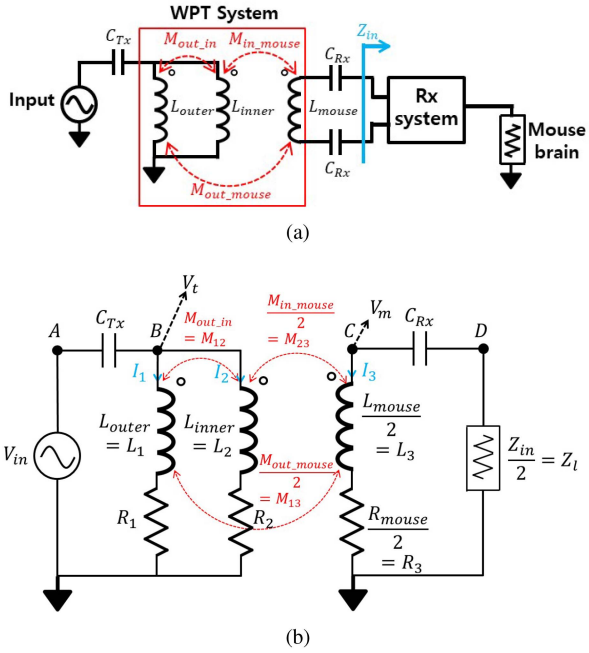

Fig. 4. The simplified schematic of the proposed WPT system (a) The diagram of the proposed WPT system (b) The simplified schematic of the proposed WPT system.

with dominant parameters, and the equivalent circuit is shown in Fig. 4(b). In Fig. 4(b), the L_{mouse}, $M_{in-mouse}$, $M_{out-mouse}$, and Z_{in} of the Rx system are divided into 2 because the middle of the Rx system designed in differential structure can be set the virtual ground. Using these parameters, Kirchhoff's current law to nodes A, B, C, and D and Kirchhoff's voltage law are applied to the circuit model. The resulting equation is shown as a matrix.

$$\begin{pmatrix} jwL_1+R_1 & jwM_{12} & jwM_{13} \\ jwM_{12} & jwL_2+R_2 & jwM_{23} \\ jwM_{13} & jwM_{23} & jwL_3+R_3 \end{pmatrix} \begin{pmatrix} i_1 \\ i_2 \\ i_3 \end{pmatrix} = \begin{pmatrix} V_t \\ V_t \\ V_m \end{pmatrix} \tag{1}$$

$$(V_{in}-V_t)\,/\left(\frac{1}{jwC_{Tx}}\right) = i_1+i_2 \tag{2}$$

$$V_{in}+\left(\frac{1}{jwC_{Rx}}+Z_l\right)\times i_3 = 0 \tag{3}$$

Furthermore, the resonance angular frequencies are calculated with the below equation [48].

$$w_0 = \frac{1}{\sqrt{(L_1||L_2)\times C_{Tx}}} = \frac{1}{\sqrt{L_3 C_{Rx}}} \tag{4}$$

Moreover, the Q-factor of the coils and coupling factors can be expressed as the self inductance, self resistance, and angular frequency. Based on the above equations, the input power, output power, and efficiency of the system are expressed as the kQ-product and calculated as the below formulas.

$$P_{in} = V_{in}\times\overline{(i_1+i_2)} \tag{5}$$

$$P_{out} = \left(\frac{Z_l}{Z_l+\frac{1}{jw_oC_r}}\right)\times V_m\times\overline{-i_3} \tag{6}$$

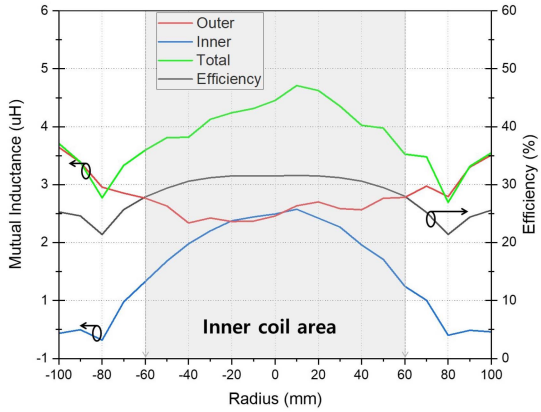

Fig. 5. The graph of the mutual inductance and efficiency along the Rx coil position.

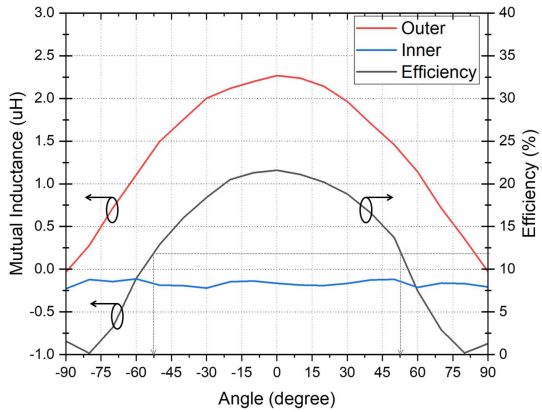

Fig. 6. The graph of the mutual inductance and efficiency along the Rx coil rotation at the 90 mm position.

$$\text{efficiency} = \frac{P_{out}}{P_{in}} \tag{7}$$

The mutual inductance of the dual coil system and the efficiency based on the kQ-product is shown in Fig. 5. The maximum value of the mutual inductance induced from the inner coil is shown in the center of the inner coil and tends to decrease as it goes to the edge of the outer coil. The measurement point is 3 cm above from the inner coil for which the position is the same as the Rx system height when the Rx module is combined with the mouse. Moreover, the mouse coil is constructed with a 3.5 cm diameter, so the mutual inductance represents the average of the magnetic fields in the mouse coil. Based on these constructions, the summation of the mutual inductance from the outer coil and inner coil to the Rx coil is maintained around 4 uH and the efficiency of the dual coil system is kept at about 30 %. Moreover, it can be confirmed that the total mutual inductance and efficiency have a flat in a 100 mm range or less value along with the variation of the Rx coil position. In other words, the power delivered to the mouse coil can be maintained almost constantly in the dual coil system. However, the dual coil system has a critical problem with Rx tilting.

Fig. 6. shows the mutual inductance of the outer coil to the mouse coil and the inner coil to the mouse coil and the efficiency

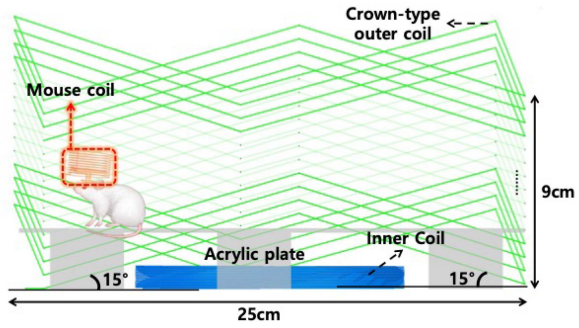

Fig. 7. The crown-type dual coil system used in the proposed WPT coil design: 3D design front view.

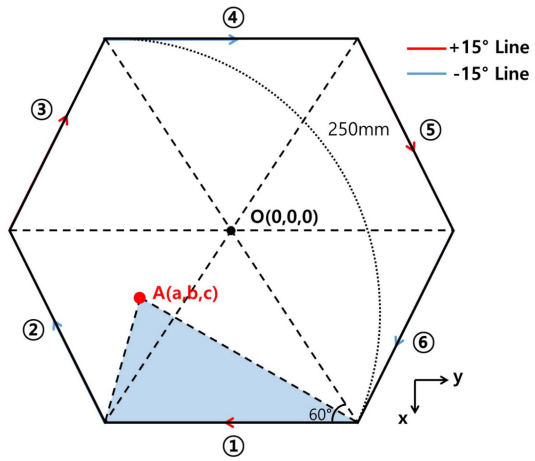

Fig. 8. Simple modeling diagram of the single closed loop coil which is part of the crown-type dual coil.

based on the kQ-product at the point with a radius of 90 mm, and the mouse coil is rotated from $-90°$ to $90°$ with a $10°$ step size. The mutual inductance of the outer coil to the mouse coil and efficiency are extremely reduced along the tilting angle. When the mouse coil is rotated about $50°$, the efficiency is reduced by half. It means that this dual coil system cannot guarantee proper power transfer about the variation angle of the mouse coil. Thus, a solution for the angle issue is still needed.

B. WPT Coil Design Using a Crown-Type Dual Coil

To solve the mouse coil tilting issue due to the movement of small animals, the design of the outer coil is changed from a circle to a crown, and the crown-type dual coil system is shown in Fig. 7. The figure shows that the crown-type dual coil has the same radius, height, and number of turns as the previous dual coil, but the coil is wound up and down by $15°$. To show that the proposed structure is more advantageous for the tilt issue due to small animal movements, the magnetic field of the crown-type coil was calculated by Matlab. For the analysis of the crown-type coil system, some parts of the design were simplified. First, the crown-type coil was modeled as a stacked straight line is shown in Fig. 8. Moreover, it is assumed that the conductor resistance of the coil is neglected; thus, the same current flows through each side, and each side is composed of a straight line.

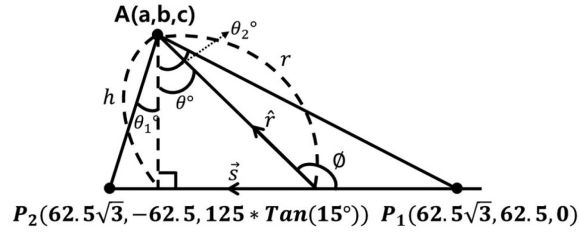

Fig. 9. Diagram of the crown-type dual coil formed by side 1 and Point A.

The magnetic field applied to the arbitrary point A from side 1 was calculated first. Fig. 9 shows the triangle formed by point A and side 1, and the coordinates of the origin O are indicated. From the Biot-Savart laws, the magnetic field induced from a finite wire is defined by (8) as follows.

$$\overrightarrow{B(r)} = \frac{\mu_0 I}{4\pi} \int \frac{d\vec{s} \times \hat{r}}{r^2} \tag{8}$$

From the cross product, the numerator can be calculated to give (9), and the direction of the $\vec{k}$ is the negative z-axis.

$$d\vec{s} \times \hat{r} = |d\vec{s}| \sin(\phi)\vec{k} \tag{9}$$

The range of the theta is from θ_2 to θ_1; thus, (8) an be transformed as follows based on the cross product.

$$\begin{aligned} \overrightarrow{B(r)} &= \frac{\mu_0 I}{4\pi h} \int_{-\theta_1}^{\theta_2} \cos(\theta) d\theta \hat{k} \\ &= \frac{\mu_0 I}{4\pi h} |\vec{s}| \times [\sin(\theta_2) + \sin(\theta_1)] \vec{u_k} \end{aligned} \tag{10}$$

This (10) can be applied to the other sides, and the summation result is calculated in MATLAB.

Fig. 10 shows the results of the normalized magnetic field analysis by MATLAB. Same as the dual coil system, most magnetic fields are formed in the negative z-axis direction. Furthermore, it was confirmed that the magnetic field is generated not only in the negative z-axis but also in the x and y axes direction following the winding direction of the crown-type coil as it approaches the edge of the coil. In Fig. 10(b) and (c), the magnetic field generated along the x and y axis affects the mouse coil when the mouse coil and the outer cage coil are misaligned due to the movement of the mouse. In other words, the tilting problem caused by the behavior of the mouse can be solved considerably due to the induced magnetic field.

In Fig. 11, the normalized mutual inductance of the dual coil and the crown-type coil is compared at 60 and 80 mm along with the rotation of the mouse coil. As shown in the figure, the difference between the dual coil and crown-type coil mutual inductance is increased when the Rx coil is positioned close to the outer coil. When the Rx coil rotated about $15°$ which angle is that the mouse head down angle, the crown-up case is larger than the dual coil case and the difference between the crown-up case and the dual coil case is bigger than the difference of the crown-down case and the dual coil case about the 60 and 80 mm both cases. Furthermore, the mouse is ensured free behavior, so the crown-up and the crown-down cases can affect the Rx coil alternately and this phenomenon can increase the

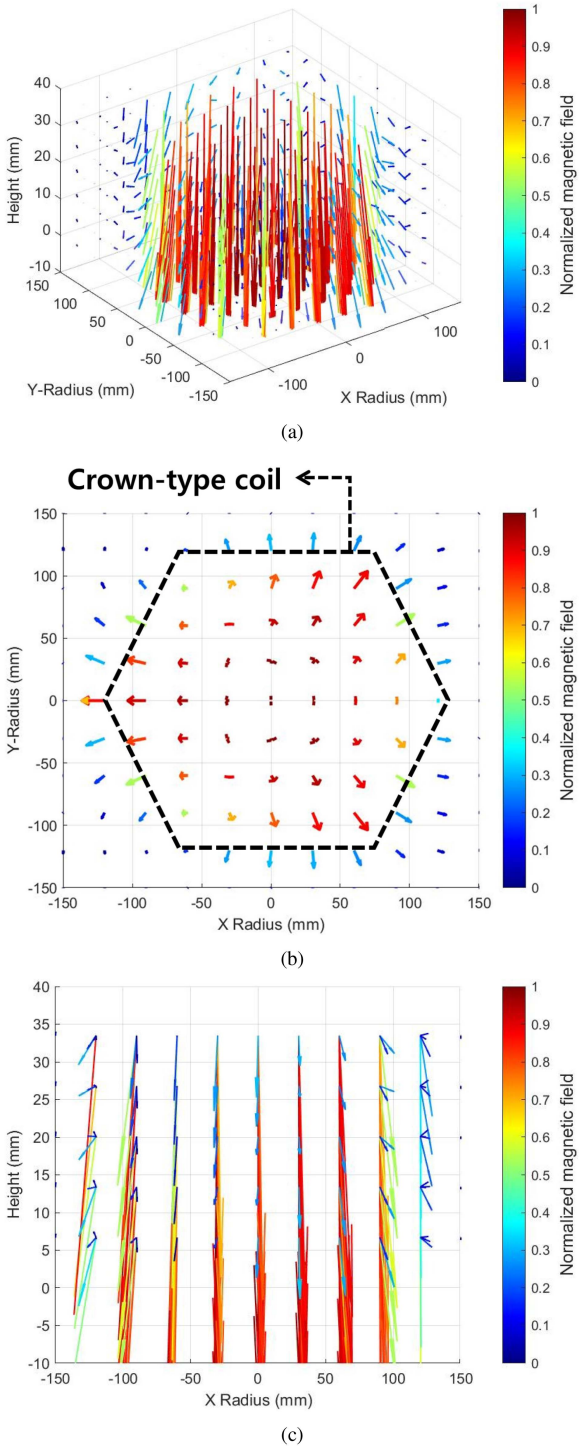

Fig. 10. The normalized magnetic field analysis result of the crown-type coil (a) Total magnetic field profile (b) Magnetic field profile at the x-y plane (c) Magnetic field profile at the y-z plane.

average mutual inductance of the crown-type coil. Based on this reason, the crown-type coil is designed to solve the misalignment issue; thus, when the Rx coil is moved close to the outer coil, the variation of the mutual inductance is insensitive to the Rx orientation. One of the characteristics of the mouse behavior is that the mouse prefers to stay close to the wall; therefore, it was

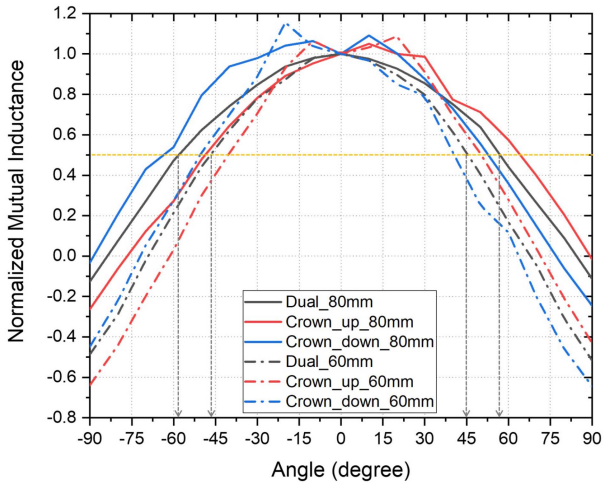

Fig. 11. The normalized mutual inductance comparison results of the dual coil and crown-type coil graph at 60 mm and 80 mm.

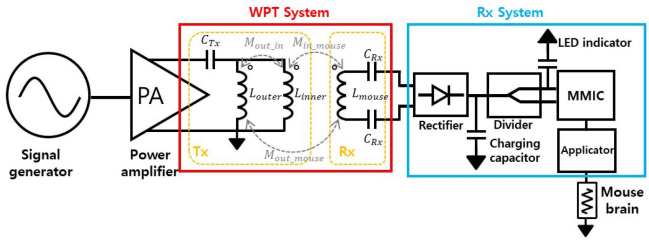

Fig. 12. Block diagram of the proposed WPT system.

confirmed that the crown-type outer coil is more robust to the orientation of the Rx system [50], [51], [52].

III. Design of the WPT System

The WPT system can be separated into two parts, the Tx and Rx parts. Fig. 12 shows a diagram of the WPT system. The Tx part consists of a signal generator for making the input AC signal and a power amplifier for amplifying the signal. The AC signal generates the magnetic field, and power is transferred to the Rx by a near-field magnetic resonance type of WPT system. To implement an efficient WPT system, the capacitors are attached to each coil so that the resonance occurs at a single target frequency of, 2.84 MHz. Then, the power transferred from the Tx is converted to DC power by the rectifier for the operation of the chip, which generates the microwave for mouse stimulation. The rectifier is constructed with 8 diodes in parallel using an applied bridge rectifier design to prevent a breakdown. The Schottky barrier diode is utilized because the diode used in the proposed system must be able to rectify a high frequency signal and yield a large current to operate the chip. The DC power is divided and supplied to the chip using a resistor voltage dividing technique for the proper driving of the chip. The resistor divider is connected with a smoothing capacitor in parallel for reducing the fluctuation of the DC voltage. The LED has the role of an indicator. It is designed to turn on the LED when the chip drives properly by connecting with the voltage divider

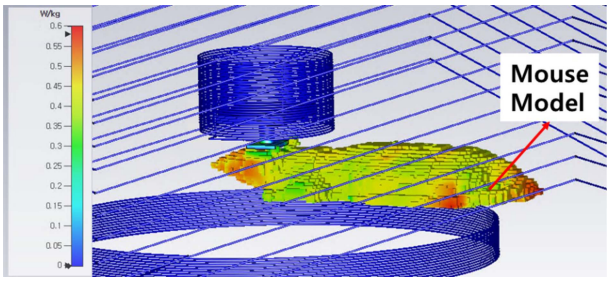

Fig. 13. The SAR simulation result of the proposed system.

taking into consideration the voltage limitation of the LED. Due to mouse movement, the LED light is sometimes blocked by the Rx coil. For this reason, the current consumption of the power amplifier is also measured to check the chip operation as well as the LED light's intensity. The mutual inductance and the amount of power transferred change by the movement of the mouse; thus, the output impedance of the amplifier also varies along the motion of the mouse. In other words, the amplifier consumes the current depending on the mouse behavior, and the operation of the chip can be checked. The chip consists of a voltage-controlled oscillator (VCO) and a power amplifier (PA) [53]. A 6.5 GHz microwave signal that stimulates the mouse is generated from the VCO, and it is amplified at PA. The chip is operated over the minimum voltage of 2.8 V, and the current is consumed at about 300 mA. For this reason, the minimum power transferred to the Rx by the WPT for operating the chip is set to 0.85 W.

It is important that the electromagnetic wave should not affects to the mouse tissues or brain. To clarify the safety of the proposed system, a specific absorption rate (SAR) simulation was done in the CST Microwave studio software. The optimized resonate capacitors are connected to the coils by lumped elements. The ICNIRP guideline states that the localized SAR values are limited to 2 W/Kg to ensure its safety. In Fig. 13, the maximum SAR value is 0.58 W/kg which is about a quarter of the guideline value, so the proposed system is confirmed to be safe from the electro-magnetic field.

IV. Measurement

A. Manual Experiment Using the WPT System

The experiment setup consisted of the Tx cage system and the Rx mouse system. The details of the Tx coils are shown in Fig. 14, and the Rx part is shown in Fig. 15. The input signal was generated by an E4438 C vector signal generator in Keysight and amplified by the ZHL-10W-202-S+ amplifier in Mini-circuit. An E3634 A power supply in Keysight supplied the voltage for operating the amplifier, and the current value was saved by the Keysight VEE program. Before attaching the Rx system to the mouse, the chip operation was verified by measuring the DC voltage using an RTO1044 oscilloscope from Rohde & Schwarz.

The Tx crown-type dual coil was wound along an acrylic cylinder with a permeability close to 1 and a diameter, height, and spacing of 250, 90, and 6 mm, respectively. The specification

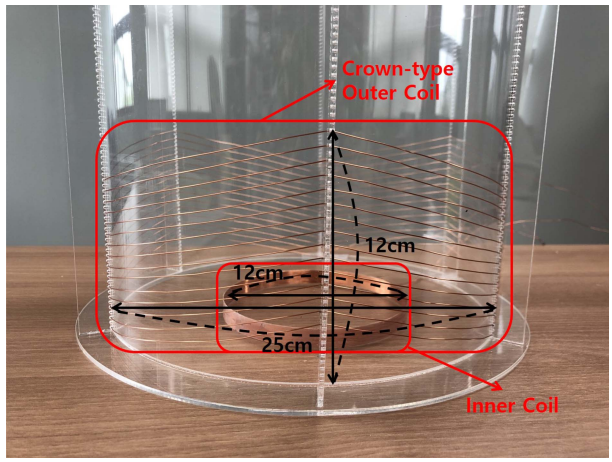

Fig. 14. Photograph of the proposed crown-type dual coil system.

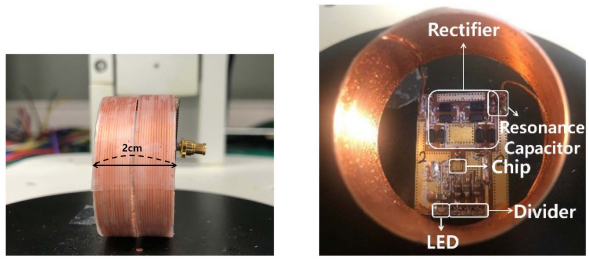

(a) (b)

Fig. 15. Photograph of the mouse coil and the Rx parts (a) Side view of the mouse coil (b) Inside view of the Rx system.

TABLE I
Specification of the Coils in the Crown-Type Dula Coil System

Parameter	Tranmitter coils		Receiver coil
	Crown-type outer coil	Inner coil	Mouse coil
Inductance (μH)	64.58	55.34	25.82
Q-factor	204.2	210.64	74.28
Diameter (mm)	250	120	35
Height	120	10	20
Number of turns	15	15	20
Conductor width (mm)	0.51	0.51	0.51

of the fabricated coils is shown in Table I. The disc shaped acrylic was placed 20 mm above the inner coil to prevent damage from the mouse. The outer coil was fixed to the 6 sidewalls attached to the acrylic cylinder. The outer coil was connected in series with the resonator capacitor (38 pF). The Tx coils and Rx coils were fabricated by UEW (Polyurethane Enamelled Copper Wire) and the diameter of the wire is 0.51 mm. The proposed Rx design was fabricated on a 2-Layer FR-4 substrate PCB shown in Fig. 15(b). The mouse coil was connected to the capacitor in series on the PCB, and the capacitance was 164 pF. The rectifier consisted of the RB162MM-40 Schottky barrier diode in the ROHM Semiconductor, and the LED used was the 19-21/R6C-AP1Q2/3 T from the Everlight Electronics corporation.

Before proceeding with the in vivo experiment, measurements were performed to verify the performance of the system. The Rx position and rotation were changed manually, and the Rx

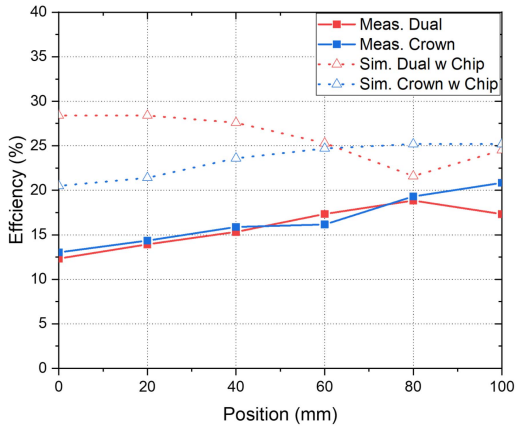

(a)

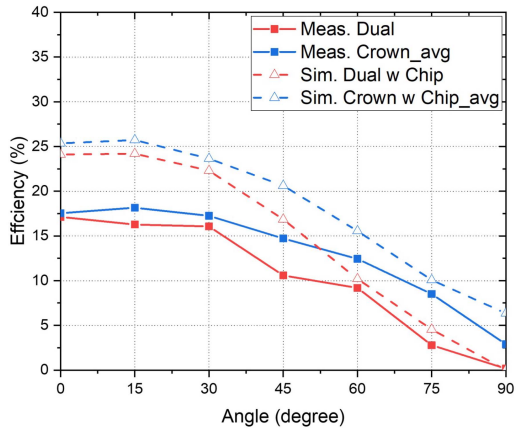

(b)

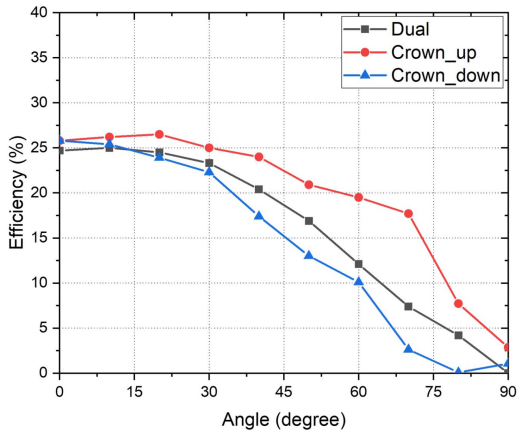

(c)

Fig. 16. The simulation and measurement results of WPT efficiency graph of the dual coil system and the crown-type system (a) The comparison graph of the WPT efficiency of the two systems along with the Rx position (b) The comparison graph of the WPT efficiency of the two systems along with the Rx angle (c) The kQ-product efficiency graph along the Rx coil orientation at 80 mm.

was positioned at 6 points and rotated from 0° to 90° with a step size of 15°. Fig. 16(a) shows that the WPT efficiency of the dual coil and the crown-type coil system along the Rx coil position. Based on the ADS and Q3D extractor simulation, the resonating capacitor is optimized but the fabrication error of the coil and the capacitor caused a decrease in the efficiency. To measure the Rx output power, an oscilloscope was used with the probe contacting the Rx system. Because of these effects, the efficiency of all systems was slightly decreased compared to the simulation results. The efficiency of the dual coil and crown-type dual coil is about 17 %. However, the minimum efficiency to operate the stimulation chip is about 8 %. Therefore, even if considering the above errors, the dual coil system, and the crown-type coil system are able to supply efficient power constantly, for operating the chip in most of the cage range.

The WPT efficiency related to the Rx system angle is shown in Fig. 16(b). The angle variation was measured at the 90 mm point where the mouse mainly stayed. As aforementioned, the crown-type outer coil has 2 different cases, one that goes up 15° and the other case that goes down 15°. The mouse is ensured free behavior, so the two cases affect the mouse coil alternatively. Therefore, the efficiency of the crown-type outer coil is measured for each case, and the average efficiency is calculated. As shown in Fig. 16(b), the efficiency of the two cases is decreased along the angle variation. However, the efficiency of the proposed system has less sensitivity to the Rx angle orientation than that of the conventional dual coil system. Especially, when the orientation angle is over the 45°, the sensitivity of the crown-type system is slightly decreased, but that of the dual coil system is extremely decreased. Based on this fact, the proposed system has an advantage in that it is more insensitive to the Rx angle variation.

The crown-type coil system was constructed for 2 cases, and in one case, it dominantly affects the Rx system and in the opposite case, it has a limited effect. Because of this reason, in one case, the efficiency was calculated mainly when it affects, and the result is shown in Fig. 16(c). When the Rx system is rotated, the efficiency of the three cases, the dual coil system, crown-type coil system that goes up 15°, and crown-type coil system that goes down 15°, decrease simultaneously. Nevertheless, the crown-up case can maintain its efficiency highly compared to the others. And the power transfer can be maximized when the Rx is tilted 20°, and it decreases along the tilting angle. Moreover, even if the efficiency of the crown-down case is lower than the dual case, the gap between the efficiency of the dual case and crown-down is smaller than the efficiency difference of the crown-up case and the dual case. Thus, the average efficiency of the crown-type system can be maintained higher than that of the dual coil system along with the Rx system orientation. Therefore, the results confirmed that the proposed crown-type dual coil is more effective to solve the issue of the orientation in the angle.

The application of this system is for an untethered mouse, and it tries to maximize the free behavior of the mouse. Therefore, when an experiment is performed, the crown-up and crown-down cases can be repeated while the mouse moves. Thus, the smoothing capacitor in the Rx system can be charged and discharged with the movement of the mouse. On the other hand, due to the RC time constant of the Rx system, the voltage will not be able to be discharged completely. For this reason, in the real stimulation experiment, the average efficiency of the crown-type dual coil system will be increased.

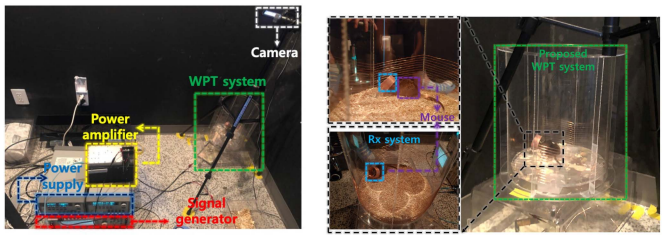

(a) (b)

Fig. 17. Experimental setup of the mouse behavior experiments. (a) Overview of the mouse behavior experiments setup (b) Photograph of the crown-type dual coil experiments setup.

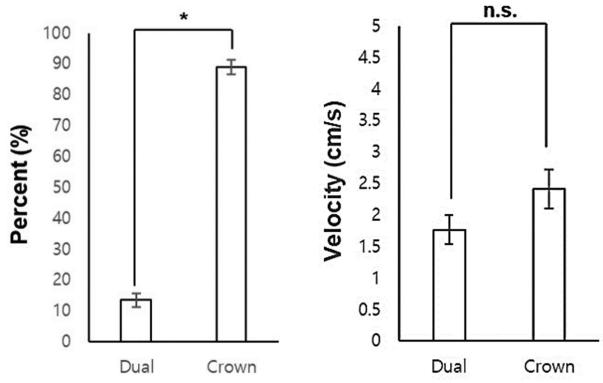

(a) (b)

Fig. 18. Graphs showing a comparison of the WPT transmitting time and mice behavior of the two types of coils (a) Graph of the WPT operation time for the 10 minutes (b) Graph showing the average velocity of the mice.

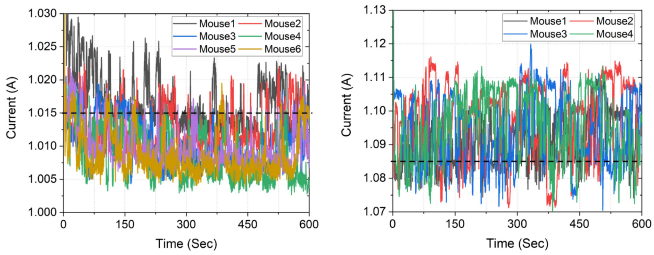

(a) (b)

Fig. 19. The current consumed by the DC supply during the behavior experiment (a) Current consumption of the dual coil for each mouse (b) Current consumption of the crown-type coil for each mouse.

B. Mouse Behavior Experiments Using the WPT System

Fig. 17 shows the experimental setup of the mouse behavior experiment. All experiments were approved and conducted according to Catholic University's Institutional Animal Care and Use Committee (IACUC) guidelines of Incheon St. Mary's Hospital (protocol numbers: CIMH-2017-003 and CIMH-2018-003). F1 hybrid male mice from C57BL/6J $\times$129/SvJae were used in the experiment. The mice were housed individually and maintained at a constant temperature (23 $\pm$ 1 °C) and humidity (50 $\pm$ 5%). All mice were housed in group cages with access to food and water ad libitum, alternating 12-hour dark-light cycles. In all experiments, all the mice were initially housed in the group cages but individually caged after the applicator surgery to protect the applicator. For the stimulation with free behavior, the applicator, which was used for matching from the brain of the mouse to the chip and transmitting the signal, was implanted into the mice. Mice older than 12 weeks were used for the WPT applicator implantation. Mice anesthetized with isoflurane (Kent Scientific, SomnoSuite) were connected to a stereotactic instrument (David Kopf Instruments, USA) for the Rx system implantation. The applicator was placed in the Bregma, and the applicator was fixed to the skull with self-tapping stainless-steel screws and dental cement (Vertex). The mice recovered for 7 days after the surgery before the experiment.

V. Result

The experiment was performed with the dual coil system and the crown-type coil system with six mice for the dual coil and four mice for the crown-type coil for about 10 minutes. Fig. 18(a) compares the WPT transmitting results of the dual coil and the crown-type coil. To compare the WPT performance of each coil during the experiment, the time when the MMIC was successfully operated was analyzed for each system. In the 10-minute behavioral experiment, the dual coil system operated for 13% of the experiment time, while the crown-type coil received power for about 90% of the experiment time (Mann-Whitney U test, p-value = 0.0105). The Rx system of the crown-type coil weighed about 0.8 grams higher than the Rx of the dual coil system due to the fabrication issues. To figure out the effect of the weight difference, the average velocity were also analyzed, and the result is shown in Fig. 18(b).

As shown in Fig. 18(b), there are no statistical differences in the average velocity between the dual coil and crown-type coil systems. Based on these results, the weight difference between the two Rx systems can be concluded to have no significant effect on the mouse behavior. In this paper, the current consumed by the DC power supply was proposed to be one way to measure the WPT performance. Through the preliminary manual test, it can be confirmed that the threshold current when the chip is operated is set to be greater than 10 mA above the minimum current. Therefore, the WPT performance can be analyzed over time, and the details are shown in Fig. 19. The graph shows the details of the current consumption of the DC power supply of each mouse over time. In the dual coil cases, the average execution time of the WPT was about 80 seconds. On the other hand, the average power transmitting time of the crown-type cases was about 530 seconds. This result shows that both the dual coil system and the crown-type coil system can transmit the power. However, the transmit time is very high in the case of the crown-type coil system compared to the dual coil system.

Based on the current consumption, Fig. 20 shows the stimulation power which can be calculated along the premeasured chip operation [54]. In the case of the conventional dual coil system, the transmitted power can drive the stimulation signal generation chip. However, the power of the stimulation signal is about 4 dBm and it is too small to get effective brain stimulation

TABLE II
PERFORMANCE SUMMARY AND COMPARISON WITH OTHER SYSTEM

	[28]	[29]	[30]	[36]	[37]	This work
Frequency	13.56 MHz	6.78 MHz	13.26 MHz	13.56 MHz	346.6 MHz	2.84 MHz
Dimension of transmitting coil (mm^3)	270 × 270 × 160	400 × 240 × 40	285 × 180 × 130	460 × 240 × 200	609.6 × 609.6 × 300	250 × 250 × 120
Dimension of receiving coil (mm^3)	20 x 20 x 10, 10 × 10 x 5	11.5 × 11.5 × 5.8	26 × 35 × 2.6	20 × 22 × 11	5 × 5, 7 × 7*2	35 × 35 × 20
Input power	250 mW	4 W*1	79 mW	2.5 W*1	2 W	10 W
PTE	20 %*3	3.8 - 7.5 %	34.1 - 41.7 %	4.1 - 33.3 %*3	1 - 10 %*1	2.9 - 19.6 %
PDL variation on XY plane	6 % *3	7.6 %	7.6 %	9.7 %	9 %*1	7.8 %
PDL	36 mW *3	100 mW*3	26.9 - 31.6 mW	40 - 43 mW*1	6.1 - 13 mW	0.3 - 1.93 W
Specification of the coils	Printed, AWG wire*1	AWG wire*1	Printed, copper tape, AWG wire	copper foil, AWG wire	Cu tape, AWG wire	AWG wire
Number of Tx and Rx coils	18 (Tx) / 2 (Rx)	2 (Tx) / 1 (Rx)	5 (Tx) / 3 (Rx)	5 (Tx) / 5 (Rx)	1 (Tx) / 2 (Rx)*4	2 (Tx) / 1 (Rx)
Simulation of SAR of the system	No	Yes	No	Yes	Yes	Yes
System Avg. operation time *in vivo* experiment	No Expt.	No Expt.	No Expt.	N/A	93.53%	89.55%

*1 Estimate from the paper *2 Biaxial arrange and diameter of the coils *3 Peak value *4 Cavity structure

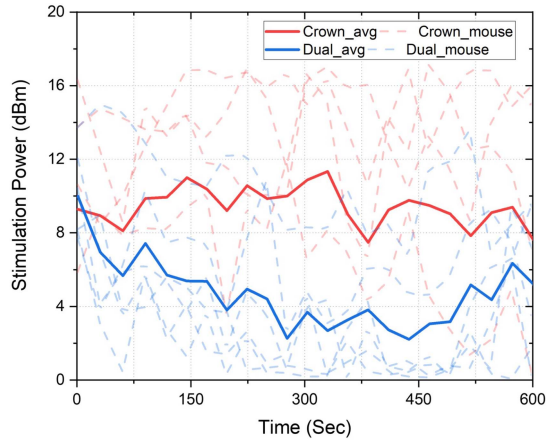

Fig. 20. Comparison graph of the stimulation power between conventional coil and crown-type coil system based on the current consumption.

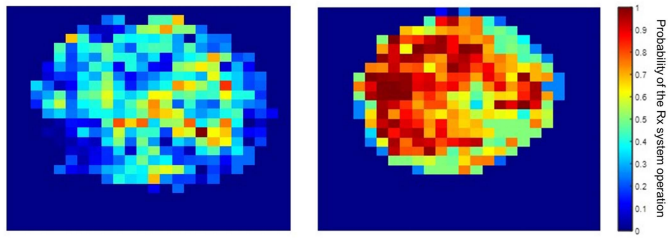

Fig. 21. The WPT performance comparison over the Rx position in the cage (a) Operation points along the Rx coil in the dual coil case (b) Operation points along the Rx coil in the crown-type coil case.

experiment results due to the misalignment issue of the system. On the other hand, the proposed crown-type dual coil system can generate twice higher power, 9 dBm, as the conventional system because the embedded coil can generate an insensitive magnetic field along the angular variation. Thus, it can be concluded that the proposed system is more practical for the free behavior animal experiment based on the WPT.

The Rx coil position in the video was tracked by DeepLabCut (DLC) for each case. The Rx coil position was trained using 60 frames from 10 randomly selected videos for 510000 iterations, and the data generated by DLC were processed using MATLAB. The Rx position data were synchronized with the consumption current, and the WPT map was plotted as the number of visits divided by the number of WPT successes for each pixel. Outlier coordinates were removed from the data, which had a difference smaller than 20 pixels per frame. The velocity and distance moved were analyzed using Ethovision X12 (Noldus), and the WPT map is shown in Fig. 21.

$$\eta_{time} = \frac{t_{op}}{t_{exp}} \tag{11}$$

The proposed system is targeted as a free behavior experiment system for mice so the system operating time also can be one parameter to evaluate this system. The time efficiency shown in (11) is calculated by dividing the total experimental time into the system operating time. Based on this parameter, the WPT performance over the Rx coil position in the cage was analyzed to compare the WPT time efficiency. According to the analysis results of the WPT execution of the two coils by location, both cases transmitted from all locations in the cage. However, the WPT time efficiency of the conventional dual coil system was not suitable due to angular issues caused by the behavioral characteristics of free movement. In contrast, the WPT time performance of the crown-type coil showed a very high efficiency because the wireless power was well transmitted to all positions in the chamber. Moreover, the WPT showed high performance during the experiment regardless of the behavioral characteristics of the free movement by the mice. In the mice experiments, the dual coil system operated for 13% of the experiment time, while the crown-type coil received power for about 90% of the experiment time. Thus, the experiment time of the proposed system is 7 times longer than the conventional system. Finally, the crown-type dual coil system solved the tilting issue shown by its high WPT performance compared to the conventional dual coil system.

VI. CONCLUSION

In this article, a highly efficient WPT system was designed to resolve the misalignment issue due to the freely moving Rx system and verified the system performance by mouse brain stimulation experiments. The system utilized MCR-WPT at the resonant frequency of 2.84 MHz and consisted of the embedded dual coil Tx system and the miniaturized Rx system.

In the Tx system, the embedded outer cage coil that looks like a crown and the solenoid type inner coil are connected in parallel. The crown-type outer cage coil is designed by repeating the

rising and falling at an angle of 15° for each side. The crown-type outer coil creates the H-field insensitive to the change in the mice orientation, and the inner coil generates a magnetic field so that the H-field is distributed uniformly along the various locations. In the Rx system, the electromagnetic power transferred by the WPT is supplied to the chip, which generates the microwave signal for the brain stimulation, by the rectifier and voltage divider. The experiments confirmed that the proposed system can operate the chip within the cage radius of 250 mm, and the chip is able to be driven during most of the experiment time and generate the stimulation signal even if the mice move freely. Therefore, the results verify that the system proposed in this paper ensures the free behavior of mice and enables more accurate animal experiments with its simple design. In Table II, the performance of the proposed WPT system is summarized and compared with that of other published work. The proposed system exhibits a high-power transfer efficiency (PTE) by using a small number of Tx and Rx coils. Furthermore, the system was verified for the stability of the mice experiment by SAR simulation, and then, mice experiments were done. As a result, the proposed system was validated showing that it is capable of a longer stimulation time during the same experiment with the small number of coils compared with the conventional system. Additionally, the proposed system will not only be applicable to various animal experiments requiring free movement but will also contribute to the development of WPT significantly. Especially, the proposed coil design can be utilized in the WPT applications which have misalignment problems and a free-positioned Rx system. In the future, the system will help to increase the efficiency of various WPT applications such as portable wireless charging, and biomedical implants and help future research on diverse animals like rats by optimizing the design of the coils.

REFERENCES

[1] A. Karalis, J. Joannopoulos, and M. Soljačić, "Efficient wireless non-radiative mid-range energy transfer," *Ann. Phys.*, vol. 323, no. 1, pp. 34–48, 2008. [Online]. Available: https://www.sciencedirect.com/science/article/pii/S0003491607000619

[2] J. Park, Y. Tak, Y. Kim, Y. Kim, and S. Nam, "Investigation of adaptive matching methods for near-field wireless power transfer," *IEEE Trans. Antennas Propag.*, vol. 59, no. 5, pp. 1769–1773, May 2011.

[3] T. C. Beh, M. Kato, T. Imura, S. Oh, and Y. Hori, "Automated impedance matching system for robust wireless power transfer via magnetic resonance coupling," *IEEE Trans. Ind. Electron.*, vol. 60, no. 9, pp. 3689–3698, Sep. 2013.

[4] H. Hong, D. Yang, and S. Won, "The analysis for selecting compensating capacitances of two-coil resonant wireless power transfer system," in *Proc. IEEE Int. Conf. Energy Internet*, 2017, pp. 220–225.

[5] W. Zhang and C. C. Mi, "Compensation topologies of high-power wireless power transfer systems," *IEEE Trans. Veh. Technol.*, vol. 65, no. 6, pp. 4768–4778, Jun. 2016.

[6] P. Shi, Y. Cao, H. Zhao, R. Gao, and S. Liu, "Parallel strips coupled split ring resonators for a desktop wireless charging system overcoming irregular route restrictions," *J. Magn. Mater.*, vol. 563, 2022, Art. no. 170005.

[7] G. Monti, M. V. D. Paolis, and L. Tarricone, "Wireless energy link for deep brain stimulation," in *Proc. Eur. Microw. Conf.*, 2015, pp. 64–67.

[8] B. M. Badr, R. Somogyi-Gsizmazia, K. R. Delaney, and N. Dechev, "Wireless power transfer for telemetric devices with variable orientation, for small rodent behavior monitoring," *IEEE Sensors J.*, vol. 15, no. 4, pp. 2144–2156, Apr. 2015.

[9] G. Monti, G. R. D. Giovanni, M. D. Liso, M. Pascali, and L. Tarricone, "Wireless power transfer strategies for medical implants: Focus on robustness and em compatibility," *IEEE Microw. Mag.*, vol. 22, no. 9, pp. 28–41, Sep. 2021.

[10] K.-J. Chen, W.-M. Chen, L.-Y. Tang, Y.-T. Cheng, M.-D. Ker, and C.-Y. Wu, "A 13.56 MHz metamaterial for the wireless power transmission enhancement in implantable biomedical devices," in *Proc. Int. Conf. Solid-State Sens. Actuators Microsyst. Eurosensors XXXIII*, 2019, pp. 1439–1442.

[11] Y. Li and V. Jandhyala, "Design of retrodirective antenna arrays for short-range wireless power transmission," *IEEE Trans. Antennas Propag.*, vol. 60, no. 1, pp. 206–211, Jan. 2012.

[12] J. Kim et al., "Development of 1-MW inductive power transfer system for a high-speed train," *IEEE Trans. Ind. Electron.*, vol. 62, no. 10, pp. 6242–6250, Oct. 2015.

[13] B. L. Cannon, J. F. Hoburg, D. D. Stancil, and S. C. Goldstein, "Magnetic resonant coupling as a potential means for wireless power transfer to multiple small receivers," *IEEE Trans. Power Electron.*, vol. 24, no. 7, pp. 1819–1825, Jul. 2009.

[14] Z. Liu, Z. Chen, and J. Li, "A magnetic tank system for wireless power transfer," *IEEE Microw. Wireless Compon. Lett.*, vol. 27, no. 5, pp. 443–445, May 2017.

[15] B. Choi, J. Nho, H. Cha, T. Ahn, and S. Choi, "Design and implementation of low-profile contactless battery charger using planar printed circuit board windings as energy transfer device," *IEEE Trans. Ind. Electron.*, vol. 51, no. 1, pp. 140–147, Jan. 2004.

[16] A. P. Sample, D. T. Meyer, and J. R. Smith, "Analysis, experimental results, and range adaptation of magnetically coupled resonators for wireless power transfer," *IEEE Trans. Ind. Electron.*, vol. 58, no. 2, pp. 544–554, Feb. 2011.

[17] G. Coté, R. Lec, and M. Pishko, "Emerging biomedical sensing technologies and their applications," *IEEE Sensors J.*, vol. 3, no. 3, pp. 251–266, Mar. 2003.

[18] A. K. RamRakhyani, S. Mirabbasi, and M. Chiao, "Design and optimization of resonance-based efficient wireless power delivery systems for biomedical implants," *IEEE Trans. Biomed. Circuits Syst.*, vol. 5, no. 1, pp. 48–63, Jan. 2011.

[19] M. Theodoridis and S. Mollov, "Distant energy transfer for artificial human implants," *IEEE Trans. Biomed. Eng.*, vol. 52, no. 11, pp. 1931–1938, Nov. 2005.

[20] R. Saha, B. R. Joy, and S. A. Mirbozorgi, "Wireless power transmission with uniform power delivery in the 3D space of the human body using resonators in parallel," in *Proc. IEEE Annu. Int. Conf. Eng. Med. Biol.*, 2021, pp. 7268–7271.

[21] A. Poon, "A new kind of wireless mouse," *IEEE Spectr.*, vol. 53, no. 12, pp. 26–32, Dec. 2016.

[22] B. Lee and Y. Jia, "Wirelessly-powered cage designs for supporting long-term experiments on small freely behaving animals in a large experimental arena," *Electronics*, vol. 9, no. 12, 2020, Art. no. 1999. [Online]. Available: https://www.mdpi.com/2079-9292/9/12/1999

[23] C. Wentz, J. Bernstein, P. Monahan, A. Guerra, A. Rodriguez, and E. Boyden, "A wirelessly powered and controlled device for optical neural control of freely-behaving animals," *J. Neural Eng.*, vol. 8, 2011, Art. no. 046021.

[24] I. Colmiais, H. Dinis, and P. M. Mendes, "WPT system for implantable devices using a phased array and tracking algorithm for freely moving rats," in *Proc. IEEE 7th Portuguese Meeting Bioeng.*, 2019, pp. 1–4.

[25] U.-M. Jow, M. Kiani, X. Huo, and M. Ghovanloo, "Towards a smart experimental arena for long-term electrophysiology experiments," in *Proc. IEEE Biomed. Circuits. Syst. Conf.*, 2011, pp. 121–124.

[26] R. Narayanamoorthi and A. Juliet, "IoT-enabled home cage with three-dimensional resonant wireless power and data transfer scheme for freely moving animal," *IEEE Sensors J.*, vol. 18, no. 19, pp. 8154–8161, Oct. 2018.

[27] S. Kamotesov, P. Lombard, V. Semet, B. ALLARD, M. Moguedet, and M. Cabrera, "The potential of 3D-MID technology for omnidirectional inductive wireless power transfer," in *Proc. Int. Congr. Molded Interconnect Devices*, Würzburg, Germany, 2018, pp. 1–6. [Online]. Available: https://hal.archives-ouvertes.fr/hal-02152067

[28] S. A. Mirbozorgi, H. Bahrami, M. Sawan, and B. Gosselin, "A smart cage with uniform wireless power distribution in 3D for enabling long-term experiments with freely moving animals," *IEEE Trans. Biomed. Circuits Syst.*, vol. 10, no. 2, pp. 424–434, Apr. 2016.

[29] J. P.-W. Chow, H. S.-H. Chung, L. L.-H. Chan, R. Shen, and S. C. Tang, "Optimal design and experimental assessment of a wireless power transfer system for home-cage monitoring," *IEEE Trans. Power Electron.*, vol. 34, no. 10, pp. 9779–9793, Oct. 2019.

[30] D. K. Biswas, J. H. A. Martinez, J. Daniels, A. Bendapudi, and I. Mahbub, "A novel 3-D printed headstage and homecage based WPT system for long-term behavior study of freely moving animals," in *Proc. IEEE Radio Wireless Symp.*, 2020, pp. 268–271.
[31] K. Eom et al., "A wireless power transmission system for implantable devices in freely moving rodents," *Med. Biol. Eng. Comput.*, vol. 52, no. 8, pp. 639–651, 2014.
[32] S. A. Mirbozorgi, Y. Jia, P. Zhang, and M. Ghovanloo, "Toward a high-throughput wireless smart arena for behavioral experiments on small animals," *IEEE Trans. Biomed. Eng.*, vol. 67, no. 8, pp. 2359–2369, Aug. 2020.
[33] S. A. Mirbozorgi, Y. Jia, D. Canales, and M. Ghovanloo, "A wirelessly-powered homecage with segmented copper foils and closed-loop power control," *IEEE Trans. Biomed. Circuits Syst.*, vol. 10, no. 5, pp. 979–989, Oct. 2016.
[34] M. Ryu, J. D. Kim, H. U. Chin, J. Kim, and S. Y. Song, "Three-dimensional power receiver for in vivo robotic capsules," *Med. Biol. Eng. Comput.*, vol. 45, no. 10, pp. 997–1002, 2007.
[35] B. Lenaerts and R. Puers, "Inductive powering of a freely moving system," *Sens. Actuator A Phys.*, vol. 123, pp. 522–530, 2005.
[36] Y. Jia et al., "Position and orientation insensitive wireless power transmission for enercage-homecage system," *IEEE Trans. Biomed. Eng.*, vol. 64, no. 10, pp. 2439–2449, Oct. 2017.
[37] H. Mei, K. A. Thackston, R. A. Bercich, J. G. Jefferys, and P. P. Irazoqui, "Cavity resonator wireless power transfer system for freely moving animal experiments," *IEEE Trans. Biomed. Eng.*, vol. 64, no. 4, pp. 775–785, Apr. 2017.
[38] J. Kim, D.-H. Kim, J. Choi, K.-H. Kim, and Y.-J. Park, "Free-positioning wireless charging system for small electronic devices using a bowl-shaped transmitting coil," *IEEE Trans. Microw. Theory Techn.*, vol. 63, no. 3, pp. 791–800, Mar. 2015.
[39] T. Lim and Y. Lee, "Reconfigurable coil array for near-field beamforming to compensate for misalignment in WPT systems," *IEEE Trans. Microw. Theory Techn.*, vol. 69, no. 11, pp. 4711–4719, Nov. 2021.
[40] C.-L. Yang, C.-K. Chang, S.-Y. Lee, S.-J. Chang, and L.-Y. Chiou, "Efficient four-coil wireless power transfer for deep brain stimulation," *IEEE Trans. Microw. Theory Techn.*, vol. 65, no. 7, pp. 2496–2507, Jul. 2017.
[41] J. Feng, Q. Li, F. C. Lee, and M. Fu, "Transmitter coils design for free-positioning omnidirectional wireless power transfer system," *IEEE Trans. Ind. Inform.*, vol. 15, no. 8, pp. 4656–4664, Aug. 2019.
[42] N. Ha-Van and C. Seo, "Modeling and experimental validation of a butterfly-shaped wireless power transfer in biomedical implants," *IEEE Access*, vol. 7, pp. 107225–107233, 2019.
[43] D. Vital and S. Bhardwaj, "Misalignment resilient anchor-shaped antennas in near-field wireless power transfer using electric and magnetic coupling modes," *IEEE Trans. Antennas Propag.*, vol. 69, no. 5, pp. 2513–2521, May 2021.
[44] R. Schill, "General relation for the vector magnetic field of a circular current loop: A closer look," *IEEE Trans. Magn.*, vol. 39, no. 2, pp. 961–967, Feb. 2003.
[45] S. Datta, "Electric and magnetic fields from a circular coil using elliptic integrals," *Phys. Educ.*, vol. 42, pp. 203–212, 2007.
[46] J. Zhao, Z. Wu, T. Yang, Y. Zhao, and L. Wang, "Electromagnetic biological effect on mice in wireless power transmission system," *IEEE Access*, vol. 8, pp. 205558–205567, 2020.
[47] T. Ohira, "The kQ product as viewed by an analog circuit engineer," *IEEE Circuits Syst. Mag.*, vol. 17, no. 1, pp. 27–32, Firstquarter 2017.
[48] K. Hata, T. Imura, and Y. Hori, "Simplified measuring method of KQ product for wireless power transfer via magnetic resonance coupling based on input impedance measurement," in *Proc. IEEE Ind. Electron. Soc. Annu. Conf.*, 2017, pp. 6974–6979.
[49] T. Ujihara, Q.-T. Duong, and M. Okada, "KQ-product analysis of inductive power transfer system with two transmitters and two receivers," in *Proc. IEEE Wireless Power Trans. Conf.*, 2017, pp. 1–4.
[50] M. L. Seibenhener and M. C. Wooten, "Use of the open field maze to measure locomotor and anxiety-like behavior in mice," *J. Visualized Experiments : JoVE*, vol. 96, 2015, Art. no. e52434.
[51] S. Park, J. Cho, and Y. Huh, "Role of the anterior insular cortex in restraint-stress induced fear behaviors," *Sci. Rep.*, vol. 12, 2022, Art. no. 6504.
[52] D. A. Christakis, J. S. B. Ramirez, and J. M. Ramirez, "Overstimulation of newborn mice leads to behavioral differences and deficits in cognitive performance," *Sci. Rep.*, vol. 2, 2012.
[53] T. Seo, S. Oh, D. Jung, Y. Huh, J. Cho, and Y. Kwon, "Noninvasive brain stimulation using a modulated microwave signal," *J. Electromagn. Eng. Sci.*, vol. 18, no. 1, pp. 70–72, 2018.
[54] S. Oh, D. Jung, T. Seo, Y. Huh, J. Cho, and J. Oh, "6.5-GHz brain stimulation system using enhanced probe focusing and switch-driven modulation," *IEEE Trans. Microw. Theory Techn.*, vol. 69, no. 9, pp. 4107–4117, Sep. 2021.

Jinhyun Kim (Graduate Student Member, IEEE) received the B.S. degree in electrical engineering from Hanyang University, Ansan, South Korea, in 2019. He is currently working toward the integrated master's and Ph.D. degrees with Seoul National University, Seoul, South Korea. His research interests include design of microwave integrated circuits and systems for 5G communication and brain stimulation.

Sanggeon Park received the B.S. degree in information and communication engineering from Inje University, Gimhae, South Korea, in 2009, the M.S. degree in brain and cognitive engineering from Korea University, Seoul, South Korea, in 2012, and the Ph.D. degree in neuroscience from the Korea University of Science and Technology, Daejeon, South Korea, in 2021. From 2012 to 2015, he was a Researcher with the Behavior and Cognitive Neuroscience Laboratory, Center for Neuroscience, Korea Institute of Science and Technology, Seoul. He has Postdoctoral experience in neuroscience and electrophysiology with Ewha Womans University, Seoul. He is currently a Research Professor with the Department of Brain and Cognitive Science, Scranton College, Ewha Womans University. His research interests include understanding the neural circuit-based mechanism of behavior, especially fear, emotion, and memory.

Seongwoog Oh (Graduate Student Member, IEEE) was born in Jeonju, South Korea, in 1995. He received the B.S. degree in electrical engineering and computer science from the Gwangju Institue of Science and Technology College, Gwangju, South Korea, in 2016, and the M.S. degree in electrical engineering from Seoul National University, Seoul, South Korea, where he is currentlyworking twoard the Ph.D. degree in electrical engineering. His research interests include design of microwave integrated circuits and systems for 5G communication and brain stimulation.

Yeowool Huh received the B.A. degree in biological chemistry from Grinnell College, Grinnell, IA, USA, in 2005, and the Ph.D. degree in neuroscience from the Korea University of Science and Technology, Daejeon, South Korea, USA, in 2014. She was a Postdoctoral Researcher with the Korea Institute of Science and Technology, Seoul, South Korea, till 2017. Since 2017 she has been a faculty member, an Assistant Professor with Catholic Kwandong University, International St. Mary's Hospital, Incheon, South Korea. Her research interests include understanding neural circuit-based mechanism of behavior, and developing neural probes for neuronal signal recording and stimulation.

Jeiwon Cho received the B.S. degree in psychology from Yonsei University, Seoul, South Korea, and the M.S. and Ph.D. degrees in neuroscience from the Rutgers–The State University of New Jersey, New Brunswick, NJ, USA. He has Postdoctoral experience in neuroscience, neurobiology, and electrophysiology with Yale University, New Haven, CT, USA, and the University of California at Los Angeles, Los Angeles, CA, USA. He is currently a Professor with the Department of Brain and Cognitive Sciences, Scranton College, Ewha Womans University, Seoul, South Korea.

Jungsuek Oh (Senior Member, IEEE) received the B.S. and M.S. degrees from Seoul National University, Seoul, South Korea, in 2002 and 2007, respectively, and the Ph.D. degree from the University of Michigan at Ann Arbor, Ann Arbor, MI, USA, in 2012. From 2007 to 2008, he was with Korea Telecom as a Hardware Research Engineer, working on the development of flexible RF devices. In 2012, he was a Postdoctoral Research Fellow with the Radiation Laboratory, University of Michigan, Ann Arbor, MI, USA. From 2013 to 2014, he was a Staff RF Engineer with Samsung Research America, Dallas, working as a Project Leader for the 5G/millimeter-wave antenna system. From 2015 to 2018, he was a Faculty Member with the Department of Electronic Engineering, Inha University, Incheon, South Korea. He is currently an Assistant Professor with the School of Electrical and Computer Engineering, Seoul National University. He has authored or coauthored more than 40 technical journal and conference papers. His research intersts include include mmW beam focusing/shaping techniques, antenna miniaturization for integrated systems, and radio propagation modeling for indoor scenarios. He was the recipient of the 2011 Rackham Predoctoral Fellowship Award at the University of Michigan. He was the Technical Reviewer for IEEE TRANSACTIONS ON ANTENNAS AND PROPAGATION and IEEE Antenna and Wireless Propagation Letters, among other journals. He was the TPC Member and as the Session Chair for the IEEE AP-S/USNC-URSI and ISAP. He has been a Senior Member of IEEE since 2017.